Analyst

Accepted Manuscript

This article can be cited before page numbers have been issued, to do this please use: D. Nodeh-Farahani, J. N. Bentley, L. Crilley, C. B. Caputo and T. C. VandenBoer, *Analyst*, 2021, DOI: 10.1039/D1AN01089A.

View Article Online
DOI: 10.1039/D1AN01089A

Paper

A boron dipyrromethene (BODIPY) based probe for selective passive sampling of atmospheric nitrous acid (HONO) indoors

Received 00th January 20xx,
Accepted 00th January 20xx

DOI: 10.1039/x0xx00000x

Danial Nodeh-Farahani, [a] Jordan N. Bentley,[a] Leigh R. Crilley,[a] Christopher B. Caputo,[a] and Trevor C. VandenBoer* [a]

People spend up to 90 % of their time indoors, and yet our understanding of indoor air quality and the chemical processes driving it are poorly understood, despite levels of key pollutants typically being higher indoors compared to outdoors. Nitrous acid (HONO) is a species that drives these indoor chemical processes, with potentially detrimental health effects. In this work, a BODIPY-based probe was synthesized with the aim of developing the first selective passive sampler for atmospheric HONO. Our probe and its products are easily detected by UV-Vis spectroscopy with molar extinct coefficients of 37863 and 33787 $M^{-1}{\cdot}cm^{-1}$, respectively, and a detection limit of 14.8 ng mL^{-1}. When protonated, the probe fluoresces with a quantum yield of 33%, which is turned off upon reaction. The synthesized BODIPY probe was characterized using NMR and UV-Vis spectroscopy. Products were characterized by UV-Vis and ultra high-resolution mass spectrometry. The reaction kinetics of the probe with nitrite was studied using UV-Vis spectroscopy, which had a pseudo-first-order rate of $k=7.7 \times 10^{-4}\ s^{-1}$. The rapid reaction makes this probe suitable for targeted ambient sampling of HONO. This was investigated through a proof-of-concept experiment with gaseous HONO produced by a custom high-purity calibration source delivering the sample to the BODIPY probe in an acidic aqueous solution in clean air and a real indoor air matrix. The probe showed quantitative uptake of HONO in both cases to form the same products observed from reaction with nitrite, with no indication of interferences from ambient NO or NO_2. The chemical and physical characteristics of the probe therefore make it ideal for use in passive samplers for selective sampling of HONO from the atmosphere.

Introduction

Nitrous acid (HONO) is a significant source of hydroxyl (OH) radicals in outdoor environments, the dominant oxidant in the ambient atmosphere. Hydroxyl radicals react with most molecules in the atmosphere, such as volatile organic compounds, to form secondary organic aerosols (SOA) and ozone (O_3). Generally, such reaction products can be detrimental to human and ecosystem health.[1-2] Although the sources and production mechanisms of atmospheric HONO are not completely understood, current knowledge can be broadly classified into homogeneous gas-phase reactions, heterogeneous surface reactions, and direct emissions.[3] Of emerging concern is the role of HONO in impacting indoor chemistry, for which we explore the utility of a BODIPY-based probe to be applied to passive gas sampling in this work.

Similar to outdoors, HONO is suspected to be a major source of OH radicals indoors.[4–6] HONO can easily photodegrade at low photon energies to form NO and OH via R1 and may dominate oxidation under natural low light conditions indoors.[7–11]

$$HONO + h\nu\ (\lambda \leq 400\ nm) \rightarrow NO + OH \qquad (R1)$$

Homogenous gas-phase reaction of NO with OH is important for production outdoors.[8,15] Heterogeneous reactions form HONO through several pathways.[12–14] Known HONO production pathways include the hydrolysis of NO_2 on wet surfaces (R2), and light-induced reactions of NO_2 on aerosols and other surfaces. The relative significance of one pathway over another is not yet well constrained.[15–17] Direct emissions outdoors include vehicle exhaust, biomass burning, and biogenic production from oxidation or reduction of reactive nitrogen by microbes in soils.[18–26] Similar loss and production pathways are expected indoors.

$$2NO_2 + H_2O \rightarrow HONO_{(g)} + HNO_{3\,(aq)} \qquad (R2)$$

To date, HONO levels indoors have been found to be substantially higher than outdoors.[27] This is of concern as inhalation of HONO can cause respiratory tract irritation and a decrease in lung capacity and function.[5,27] Studies to date have measured HONO mixing ratios in indoor

[a] Department of Chemistry, York University, Toronto, Ontario M3J 1P3, Canada.

Electronic Supplementary Information (ESI) available: [details of any supplementary information available should be included here]. See DOI: 10.1039/x0xx00000x

View Article Online
DOI: 10.1039/D1AN01080A

environments with an average near 5 parts per billion by volume (ppbv), while 24-hour average outdoor levels in North America have mixing ratios below 1 ppbv.[4,6,27–32] In an indoor environment, HONO can be emitted via combustion sources such as candles, gas stoves or cigarette smoke. These sources release HONO in equal amounts to NO_x; reaching tens to hundreds of ppbv mixing ratios which are a concern for inhalation exposure.[6,28,33] Surface conversion of NO_2 to HONO on hydrated or acidic surfaces is also suspected to be important.[5,34–37] In addition, sources of amines are higher indoors, particularly in smoking households, and the reaction of HONO with secondary and tertiary amines (R3) forms carcinogenic nitrosamines. Thus it is crucial to understand the controls on HONO chemistry and levels in indoor environments.[38,39] It is also important to develop safe and non-intrusive methods capable of quantifying indoor HONO at ppbv levels or lower.

$$HONO + (R)_2NH \rightarrow (R)_2NNO + H_2O \qquad (R3)$$

Instruments commonly used for measuring outdoor HONO could be considered unsafe, intrusive, or disruptive to occupants, whose unperturbed activities are necessary for understanding indoor chemical transformations. Such instruments include chemical ionization mass spectrometry (CIMS)[24,31,40], long path absorption photometry (LOPAP) [14,41,42], online ion-chromatography systems, and differential optical absorption spectroscopy (DOAS). [11,13,43] All require expert operators and have space, power, or safety restrictions that preclude their routine application in indoor environments. Those using toxic chemicals, reagents, and radioactive sources are unsafe or logistically impossible to introduce around occupants in indoor environments to study relevant chemistry driven by their typical activities. Perhaps the most important limits are the costs of purchasing and running one of these instruments, limiting the capability to make simultaneous measurements in many different locations. Obtaining a large statistical pool of observations with research grade instrumentation is therefore challenging, yet crucial, in surveys of indoor air composition as well as exposure studies.

Passive sampling provides the bridge between detailed observations and large surveys. They are time-integrated collectors of target gases that diffuse to their surface, followed by reaction or partitioning into the sampling substrate. The passive analyte collection is generally followed by aqueous extraction and offline measurements of the collected molecule(s). Passive samplers are reproducible, silent, cheap, and simple to use.[44,45] They do not need a power source or any field calibration, making them ideal for use in remote and indoor environments.[44,46,47] They selectively sample the analyte of interest through targeted reaction chemistry, yielding a stable analyte in a predictable matrix and a small volume of extraction solvent. Passive samplers combine active air sampling protocols into one step, which simplifies storage and transport. Lastly, they can detect lower quantities of an analyte gas by merely increasing their sampling time.[45] Due to these advantages, the technique is typical for NO_x ($\equiv NO_2 + NO$) and NO_2 measurements in indoor and outdoor environmental surveys where large numbers of measurements are required.[4] In this work, we extend this strategy to the sampling of HONO. This comes with the added benefit that HONO measurements allow targeted samplings of nitrogen oxides to be corrected for known positive bias due to HONO interference.[48] Mitigating this bias is critical to ensuring reliable measurements of these regulated reactive gases indoors. Taken together, these needs justify the development of the first selective passive sampling measurement for HONO.

4,4-Difluoro-4-bora-3a,4a-diaza-s-indacene (BODIPY) are a class of popular fluorescence probes especially in the field of bioimaging for labelling proteins and DNA.[49,50,51] They are also ideal for use in passive sampling. This is mainly because of their high molar absorptivity coefficients and high fluorescence quantum yields.[52] However, few water-soluble BODIPY probes have been reported; a necessary property to be of use under environmental conditions or extraction and dissolution into aqueous media.[53,54]

Since nitrite is present in the human body, wastewater, and many other systems, highly absorptive and/or fluorescent molecular probes for nitrite detection have been reported.[55,56] Thus, some BODIPY based probes have been developed to quantify nitrite.[55] However, attempts to sample and detect its conjugate acid (HONO) has never been done before.[57,58] This suggests that BODIPY probes could be effective in addressing the current limits of HONO passive sampling in indoor environments, but this has not yet been demonstrated. The development of a selective and sensitive HONO probe that is amenable to aqueous environments and stable for quantitation remains to be explored.

Herein, we synthesized a water-soluble amino-BODIPY probe that reacts with both nitrite and HONO. The optical properties of the molecule were characterized. We quantified the reaction rate of the probe with nitrite and characterized the reaction products for quantification. Proof-of-concept experiments with calibration gas sources of HONO demonstrate the utility of our probe for application to passive sampling.

View Article Online
DOI: 10.1039/D1AN01089A

Experimental

Reagents and instruments

Commercially available chemicals were purchased from either Sigma-Aldrich (Burlington, ON, CA), TCI Chemicals (Portland, OR, USA), or Oakwood Chemicals (Estill, SC, USA) and employed without further purification; unless otherwise stated. In house 18.2 MΩ·cm Milli-Q® Water Purification System (Milli-Q® Direct 8, Millipore Sigma, MA, USA) were used to obtain deionized water (DIW).

Emission and excitation measurements were recorded with a fluorescence spectrometer (Model FS5, Edinburgh Instruments Ltd, UK). Emission spectra were excited at the respective absorption maxima unless stated otherwise. Ultraviolet-visible (UV-Vis) measurements were recorded with either a Cary 5000 UV-Vis-NIR Spectrometer or Ocean Optics Flame spectrometer FLAME-S-XR1-ES (Gamble Technologies Limited, ON, CA). Recordings were obtained at 25 °C and taken with the instrument operating in single beam mode. Quantum yield measurements were performed by switching the cuvette holder to an SC-30 Integrating Sphere holder (Edinburgh Instruments Ltd, UK) on the Edinburgh FS5 instrument. All measurements were referenced to deionized water, as the solvent. All absorption and fluorescence experiments were conducted in quartz cuvettes (1 cm x 1 cm) sealed with a threaded PTFE cap (Spectrosil®23-Q-10, Starna Scientific, UK).

Experiments monitored by NMR spectroscopy were conducted in NMR spectrum tubes (8" x 5 mm) sealed with standard plastic caps and wrapped with Parafilm or J-young screw cap. ^{1}H, ^{11}B, $^{13}C\{^{1}H\}$, $^{19}F\{^{1}H\}$ NMR spectra were acquired at 25 °C on either a Bruker 700 MHz, DRX 600 MHz, ARX 400 MHz, or ARX 300 MHz Spectrometers. Chemical shifts are reported relative to $SiMe_4$ and referenced to the residual solvent signal (^{1}H, $^{13}C\{^{1}H\}$) of $CDCl_3$ (δ 7.26, 77.16 µg/mL) or C_6D_6 (δ 7.16, 128.06 µg/mL). ^{11}B and $^{19}F\{1H\}$ NMR spectra were referenced relative to 15% BF_3-Et_2O. NMR spectra were analyzed using either TopSpin 4.0.1 (Bruker Corporation, Milton, ON, Canada) or MestReNova 12.0.3-21384 (Mestrelab Research, Spain) software. Data analysis and graphics were generated using WaveMetrics Igor Pro 8.04 (Portland, OR, USA).

Synthesis

A detailed description of the synthesis for the 2,6-disodiumsulfonyl-1,3,7,9-tetramethyl-5-(4-aminophenyl)-BODIPY (BODIPY-NH_2), which is a known compound, used in this work is presented in the Supporting information.

NMR for 2,6-disodiumsulfonyl-1,3,7,9-tetramethyl-5-(4-aminophenyl)-BODIPY (BODIPY-NH_2)

The following observations were obtained from the NMR measurements. **^{1}H NMR** (400 MHz, Methanol-d4) δ 7.00 (d, J = 8.4 Hz, 1H), 6.90 (d, J = 8.4 Hz, 1H), 2.80 (s, 4H), 1.84 (s, 4H). **^{11}B NMR** (128 MHz, Methanol-d4) δ 0.73 (t, J = 32.1 Hz). **^{13}C NMR** (101 MHz, Methanol-d4) δ 155.87, 151.03, 148.42, 143.55, 135.52, 132.35, 130.00, 123.91, 116.60, 14.38, 13.80. **^{19}F NMR** (377 MHz, Methanol-d4) δ -144.46 (dd, J = 64.3, 31.8 Hz). The data was in agreement with literature, confirming that our probe was pure and could be interrogated for its optical and chemical properties.[53] Fig 1 shows the synthesis pathway for the BODIPY-NH_2 probe. NMR spectra of BODIPY-NH_2 are shown in Figs S9-12.

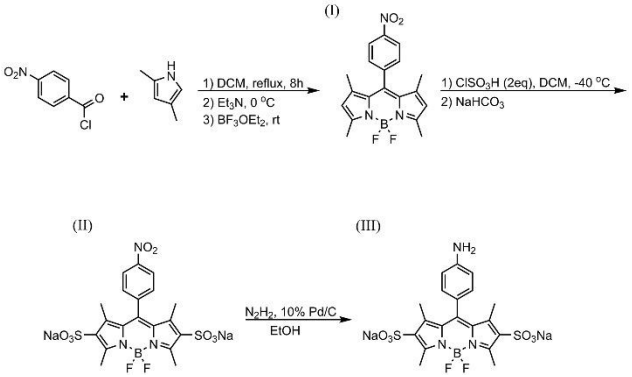

Fig 1. BODIPY-NH_2 synthesis scheme

Preparation of BODIPY-NH_2 and nitrite solution for reaction

A stock solution of BODIPY-NH_2 was made by dissolving 3.1 mg of its crystal (NewClassic MS, Mettler Toledo, ON, CA) in DIW using a 100 mL Pyrex volumetric flask. The nitrite (NO_2^-) solution for each experiment was made daily by dissolving 19.6 mg of its sodium salt in DIW using a 50 mL Corning™ Class B polypropylene volumetric flask with tapered polypropylene stopper. This stock solution was diluted to reach a NO_2^- concentration 10 times greater on a mole basis than the BODIPY-NH_2 to carry out reactions. To facilitate the reaction, one drop of concentrated HCl (34-36%) was added to 1.5

mL of BODIPY-NH_2 solution to generate BODIPY-NH_3^+.

Sampling gaseous HONO with BODIPY-NH_3^+

A solution of BODIPY-NH_3^+ collected HONO at ppbv mixing ratios for three days via bubbling in an unfritted-impinger (CG-1820-01, 04, and -10, Chemglass Life Sciences, Vineland, NJ). The sampled HONO was produced at 100 sccm from a calibration source, according to the method of Zhou et al.[4] The BODIPY-$NH_3^+$was made by diluting 5 mL of 314.8 µg/mL BODIPY-NH_2 with 5 mL of concentrated HCl and DIW in a 50 mL volumetric flask, then transferring 25 mL of the solution to the impinger. The gas flow exiting the bubbler was diluted with zero air (8301 Series Zero Air Generator, American Ecotech, Warren, RI, USA) to 1000 sccm to meet the flow requirements of a Serinus EC9841 NO_x analyzer (American Ecotech) demonstrated previously to quantitatively measure HONO.[4] The bubbler was bypassed to conduct negative controls by supplying zero air and positive controls of HONO from the calibration source. A schematic of the experimental setup is provided in Fig S14.

Mass spectrometry characterization of the reaction product

The reaction product was directly infused into an electrospray ionisation source that was operated in negative ion mode on an Agilent 6538UHD Q-TOF MS (Agilent Technologies, CA, USA). Analysis was performed on three samples: i) 2.5 mL of 314 µg/mL BODIPY-NH_3^+as an unreacted sample, ii) 2.5 mL of 314 µg/mL BODIPY-NH_3^+ reacted with 0.5 mL of 2360 µg/mL $NaNO_2$, and iii) the resulting solution obtained after bubbling HONO in BODIPY-NH_3^+.

Results and Discussion

Optical properties of BODIPY-NH_2 upon reaction with NO_2^-

The absorption maxima of the probe (BODIPY-NH_2), the conjugate acid (BODIPY-NH_3^+), and the product(s) after reaction with NO_2^- were measured by UV-Vis and determined to be 496 nm, 500 nm, and 506 nm, respectively (Fig 2). There is a 10 nm difference between the absorption maxima of BODIPY-NH_2 and the product of the reaction indicating that the product is sufficiently resolved to be detected by UV-Vis in a mixture. The molar absorptivity coefficients of BODIPY-NH_2, BODIPY-NH_3^+, and the product were measured using absorbance profiles from a range of solution concentrations (Fig S15) and were calculated to be 37860 ± 3200 M^{-1} cm^{-1} (λ=496 nm, n=4, 1σ standard deviation), 38200 ± 3570 M^{-1} cm^{-1}, (λ=500 nm, n=4, 1σ), and 33790 ± 1900 M^{-1} cm^{-1} (λ=506 nm, n=4, 1σ), respectively. The BODIPY-NH_2 showed stability over 8 months of storage in aqueous solution which was acidified to produce BODIPY-NH_3^+ prior to the measurement (Fig S16). When HCl was added to the BODIPY-NH_2 the amino some of the sulfonate groups may have been protonated. Protonation of the nitrogen lone pair converts the donor substituent to an acceptor, which in turn, bathochromically shifts the optical properties and improves the fluorescence quantum yield.

The optical properties of the reaction product are suitable for quantitative analysis where fluorescence detectors are not available or monitoring the loss of BODIPY-NH_2 would be inaccurate. To this end, we forced a reaction of BODIPY-NH_2 to completion with 10 times excess NO_2^- on a molar basis.

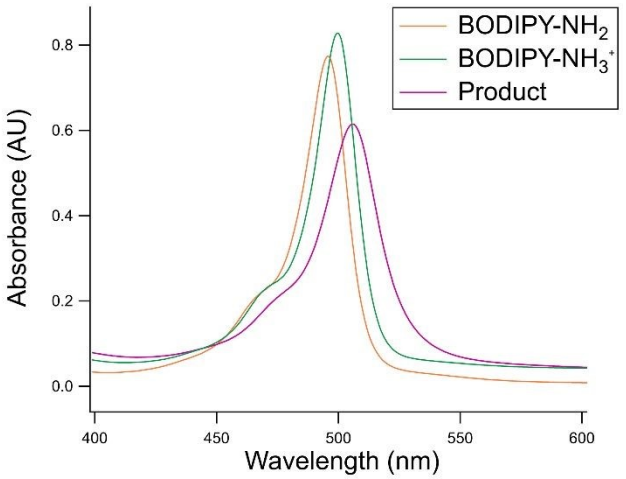

Fig 2. Absorbance of 15.5 µg/mL solutions of BODIPY-NH_2, BODIPY-NH_3^+, and the product of reaction between BODIPY-NH_3^+ and excess nitrite measured with Edinburgh FS5.

After reaction with NO_2^-, it was observed that the product colour visible by eye to be different than that of either BODIPY-NH_2 or BODIPY-NH_3^+. No fluorescence was detected for the reaction product.

View Article Online
DOI: 10.1039/D1AN01089A

Quantum yields for photons emitted between 475-700 nm for the BODIPY-NH_2, BODIPY-NH_3^+, and product of the reaction, are 1% (λ_{ex}=495 nm), 33% (λ_{ex}=495 nm), and 0% (λ_{ex}=512 nm), respectively (see Fig S17 for emission spectra). Since the BODIPY-NH_3^+ can be clearly discerned by its intense emissive properties, it shows that this molecule could act as a fluorescent ON-OFF sensor for NO_2^- detection by measuring the fluorescence decay signal. The molar absorption coefficient of the product remaining very high means the use of BODIPY-NH_2 as a sensor could detect low quantities of NO_2^- and/or HONO. The best quantitative performance would be expected where the product can be separated from the probe, prior to detection by UV-Vis. To gain insight into how this might be carried out, we analysed a sample of the reaction product to determine its sensitivity in our simple UV-Vis system and then by mass spectrometry to discern its structure.

Sensitivity of the probe

The sensitivity of the probe was determined by analysing a series of varying concentrations of the reaction product. The absorbance was measured with our UV-Vis Ocean Optics Flame spectrometer with a 1 cm path length. Measured absorbance was plotted against concentration (Fig S18) and the limit of detection (LOD) calculated as three times the standard error of the slope divided by the slope. Based on a 1:1 mole ratio between reaction of BODIPY-NH_3^+ and HONO, the LOD for the probe was determined to be 14.8 ng mL^{-1} of HONO in solution. We note that this calculated LOD is specific to this instrument and would improve by increasing the path length and spectral resolution.

Characterization of the products of the reaction of probe with HONO and $NaNO_2$

The products of the reaction of BODIPY-NH_3^+ with excess $NaNO_2$ in acidic solution were detected at 483.07, 499.06, and 517.03 amu. For the reaction of BODIPY-NH_3^+ with the gas-phase HONO (see below), the same three products were observed, suggesting a similar pathway for both reactions. The detection of products with m/z 499.06 and 517.03 is consistent with the reactions proceeding via nitrosonium formation. The protonation of NO_2^- to HONO is followed by the reaction of nitrosonium and BODIPY-NH_2 to form the nitrosamine, and finally, this forms a diazonium salt. The diazonium salt is unstable and readily loses N_2 and the molecule undergoes additions as shown in Fig 3. This chemistry is well established and exploited in other reactions that detect NO_2^- in environmental samples.[56,59]

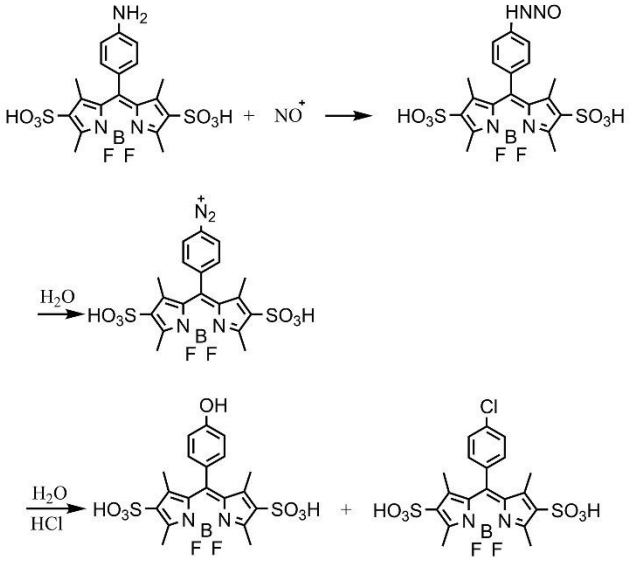

Fig 3. Proposed pathway from the reaction of BODIPY probe with nitrite and HONO to products with m/z of 499.06, and 517.03 amu

These products were confirmed with mass spectrometry, and the presence of the boron atom in our BODIPY probe allows the use of isotopic patterns when isolating the reaction product from the sample solution. Three samples: a protonated BODIPY-NH_3^+ as an unreacted sample, the BODIPY-NH_3^+ reacted with excess $NaNO_2$, and the BODIPY-NH_3^+ bubbled with gaseous HONO were analysed. The collected mass spectra are provided in Figs S19-21. The three ions with mass to charge ratios (m/z) of 499.06, 517.03, and 483.07 contained the boron isotopic pattern indicating the presence of part of the BODIPY core in the reaction products. The ion with m/z 499.06 corresponds to the presence of a hydroxyl group in place of the amino on the BODIPY-NH_2 probe. The ion with m/z 517.03 corresponds to the presence of a chlorine substituent, and at m/z 483.07 a hydrogen in place of the amino on the BODIPY-NH_2, respectively.

The unreacted sample had two ions present in the mass spectra: a dominant peak at m/z 498.08 corresponding to BODIPY-NH_2 (Fig S19), and another peak at m/z 483.07 with roughly 40 times lower intensity. Sodium and chloride adducts of BODIPY-NH_2 were also observed.

The products of the reaction of BODIPY-NH_3^+ with excess sodium nitrite had three abundant ion peaks in the mass spectra at m/z of 483.07, 499.06, and 517.03 with relative intensities of 26%, 27%, and 47%, respectively. The product of BODIPY-NH_3^+ bubbled with gaseous HONO had the same three

View Article Online
DOI: 10.1039/D1AN01089A

peaks in its mass spectra at m/z of 483.07, 499.06, and 517.03 with relative intensities of 43%, 22%, and 35%, respectively. In both product samples, there was no peak detected corresponding to the BODIPY-NH_2 probe at m/z of 498.08, meaning that the reaction in both samples went to completion, or at least far enough so as to be undetectable by this instrumental technique. In order to provide extra assurance that the ions detected correspond to the structures shown in Fig 4., the ions at m/z 483.07, 499.06, and 517.03 were selected for high-resolution accurate mass analysis and processed with the molecular formula software algorithm in MassHunter Qual B.06.00 (Agilent Technologies, CA, USA) to confirm the atomic formulas.

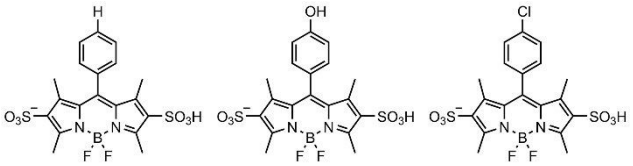

Fig 4. The products of the BODIPY-NH_2 reaction with nitrite and HONO determined from high resolution accurate mass analysis with m/z of 483.07, 499.06, and 517.03 amu from left to right

Kinetics of the reaction

We investigated the rate of the reaction between our BODIPY-NH_2 and NO_2^- in acidic aqueous solution. This was carried out under pseudo-first-order conditions with 10 times molar excess of nitrite. Spectra were acquired every minute over the 10-minute reaction time. The first spectrum was gathered immediately after the NO_2^- was added to the BODIPY-NH_3^+ solution. A shift in maximum absorption was observed from 500 nm to 506 nm. This indicates that the product(s) of reaction between NO_2^- and BODIPY-NH_3^+ formed and the reaction had proceeded to completion (Fig 5). Which of the three, or combination thereof, detected by MS dominates in these experiments was not possible to discern and will be the focus of future work. The reaction was complete in under 10 minutes. An isosbestic point at 505 nm shows the transition from BODIPY-NH_3^+ to product(s) happened without forming any long-lived intermediates. Assuming a pseudo-first-order reaction, the rate of reaction could be calculated ($k=7.7\times10^{-4}$ s^{-1}; Fig S22), resulting in an upper limit for the second order rate of 1.33 M^{-1} s^{-1} for our experimental concentration of nitrite. The rate of reaction is fast enough that even at a 1:1 mole ratio of NO_2^- to the probe, the reaction would to be complete in minutes. To apply any sampling probe to the collection of HONO from indoor air, such a fast and effective reaction is required. This is particularly true for passive sampling where collisions between the analyte gas and the probe molecule fixed to the surface initiate the reaction sequence. The rapid rate of reaction observed in solution provided sound evidence that our probe was suitable to test for its ability to react with gas-phase HONO from a calibration source.

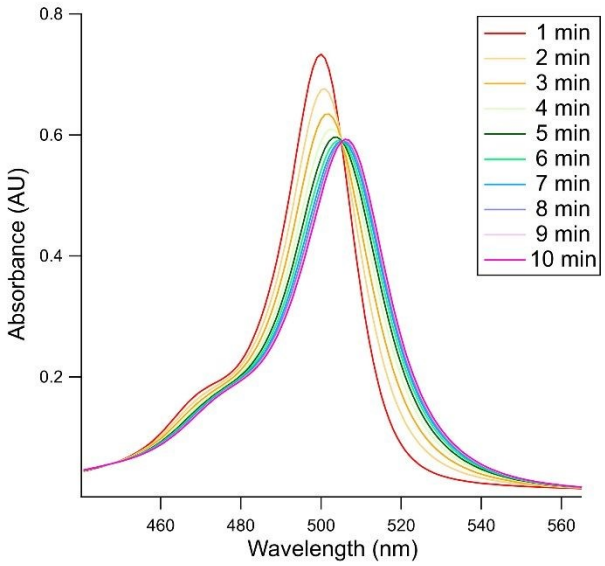

Fig 5. Changes in absorbance of 15.5 mg L^{-1} BODIPY-NH_3^+ in acidified aqueous solution with 10 times molar excess nitrite at pH 0, recorded at 1-minute intervals over 10 minutes measured with Edinburgh FS5.

Sampling gaseous HONO with BODIPY-NH_3^+

Initial testing of BODIPY-NH_3^+ to sample gaseous HONO was carried out using atmospherically relevant mixing ratios (2-4 ppbv). The HONO was produced from a calibration source as described in Lao et al.[60] The HONO was sampled for eleven days so the reaction could reach completion. When HONO was bubbled into the BODIPY-NH_3^+ solution, the mixing ratio decreased dramatically (90-100%). This suggested that HONO reacted rapidly with the available BODIPY-NH_2 in the acidified solution.

HONO is expected to form the nitrosonium cation in acidic solutions, as shown in Fig 3. Thus, 1 M HCl was selected as a non-oxidizing source of hydronium ion, enabling efficient conversion of HONO to nitrosonium at a pH near zero. The nitrosonium cation reaction with aromatic amines would follow the diazonium pathway and form some of the products observed by MS (Fig 3).[59] An advantage of

sampling into aqueous solution with a pH near zero is to maintain the protonation of the amino group on the BODIPY-NH_2. This limits the reactivity of the amino group toward addition at electrophilic sites and minimizes the decomposition of the BODIPY probe.

The reaction of BODIPY-NH_3^+ with HONO (Fig 3) was confirmed by the observation of a shoulder in the UV-Vis product spectrum (Fig 6). Unexpectedly, the decreased absorbance observed by UV-Vis indicated either decomposition or physical loss mechanisms were present. We expected the absorption maxima to shift (as observed in Fig 5), but not that the integrated absorbance would decrease (Fig 6). This is because the molar extinction coefficients of the precursor and product were determined to be similar (~35000 $M^{-1}cm^{-1}$). We hypothesized that the additional loss could be due to the apparatus (e.g. the sintered glass frit of the impinger) and/or physical removal of the probe in the form of aerosols which could be generated by bubbles bursting. To explore this loss mechanism further, we performed a negative control experiment in which we bubbled a solution of the probe with only ultrapure nitrogen gas at the same flow for eight days. We observed a 30% loss in absorption (Fig S23), suggesting that during this first HONO sampling experiment (Fig 6) the probe was lost by some mechanism(s) attributable to the experimental setup alone. This prevents reaction characterization by a mass balance approach (see below). Therefore, to minimize loss of the probe in future experiments we used a non-fritted impinger and reduced the sampling time by utilising higher HONO mixing ratios. Modification of the HONO calibration source to generate these higher mixing ratios was achieved with 1 g of dispersed sodium nitrite salt instead of a coated sodium nitrite reactor, according to Zhou et al.[4]

To differentiate between the different uptake mechanisms possible in our sampling setup, a series of control experiments were designed in which HONO was bubbled through i) deionized water (DIW), ii) 1 M HCl, and iii) 4.96 µg mL^{-1} aniline solution in 1 M HCl (Fig 7). Aniline was chosen because of the similarity of the reaction of aromatic amines with HONO to form diazonium salts. The NO, NO_2, and HONO temporal trends in these experiments were recorded at 1-minute intervals using a modified NO_x analyzer (see methods).

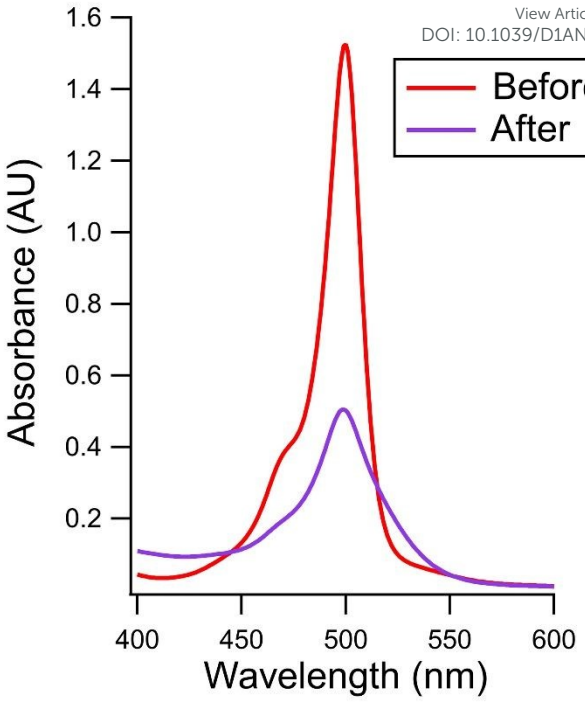

Fig 6. Changes in absorbance of the BODIPY-NH_3^+ before and after bubbling with 3.5 ppbv of HONO for a period of 11 days measured with Edinburgh FS5.

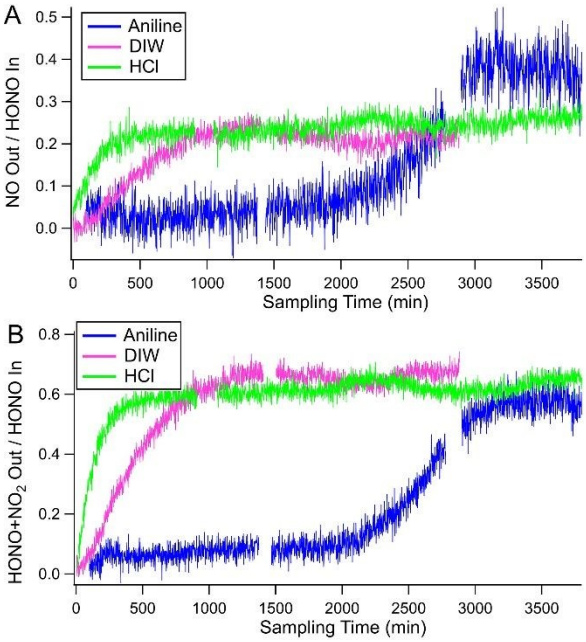

Fig 7. Time series of NO_x measurements from the exit of the impinger when gaseous HONO is bubbled into deionized water (DIW, pink), 1 M HCl (green), and 4.96 µg mL^{-1} aniline in 1 M HCl (blue). (A) The fraction of NO generated relative to HONO sampled from the calibration source and (B) the fraction of measured HONO + NO_2 relative to the same HONO input. Curve inflections indicate equilibration,

View Article Online
DOI: 10.1039/D1AN01289A

breakthrough, and/or production of the detected gases.

From Fig 7B, similar temporal trends in HONO + NO_2 output relative to the HONO delivered were observed when the impinger contained 1 M HCl and DIW, suggesting that there was little difference in the chemical uptake of HONO between these solutions (R4). As expected, there is less holding capacity for HONO in these solutions in the absence of chemical reaction with either aniline or BODIPY-NH_3^+ and the HONO would start to decompose in solution into NO and NO_2 through R5.

$$HONO_{(aq)} + H_2O \leftrightarrow H_3O^+_{(aq)} + NO_2^-{}_{(aq)} \quad (R4)$$

$$2HONO_{(aq)} \rightarrow NO_{(g)} + NO_{2\,(g)} + H_2O \quad (R5)$$

Aniline was expected to undergo the same diazotization pathway as proposed for our BODIPY-NH_3^+ probe when bubbled with gaseous HONO according to R6:

$$C_6H_5NH_2 + HONO_{(aq)} \rightarrow C_6H_5OH + H_2O + N_{2\,(g)} \quad (R6)$$

A different trend in the ratio of the HONO + NO_2 exiting the impinger solution compared to HONO input was observed for the aniline solution (Fig 7B). The fraction was persistently low (<10%) for the first 2000 mins (Fig 7B). The absence of HONO and NO_2 in the outflow of the bubbler containing the acidic aniline solution indicates quantitative and irreversible chemical loss, as expected for this positive control. After approximately 2200 minutes of sampling, the fractions of both HONO + NO_2 and NO in the outflow of the bubbler were observed to increase (Fig 7), pointing to a reduction in available aniline for reaction with HONO. At this point, $1.27(\pm0.38)\times10^{-6}$ moles of HONO had been sampled, which was 95±30% of the available aniline (1.33×10^{-6} moles) in the solution, consistent with the error resulting from the 10-30% precision of the modified HONO source.[60] This indicates that the reaction of HONO and aniline (R6) was near or beyond completion and that the experimental setup was valid for mass balance experiments. A detailed treatment of the mass balance calculation is available in the Supporting Information (Section S2). In all control experiments, a steady state in the levels of NO and NO_2 were observed in the air exiting the bubbler solution. In the negative controls, this was reached once they had equilibrated, or in the positive control, when the aniline was reacted to completion (Fig 7). The earlier observation of this rise in NO and NO_2 levels was due to the reduced chemical uptake for HONO (R6) in 1 M HCl and DIW. Thus, the sum of measured NO and HONO + NO_2 (in the absence of R6) should be equal to the HONO delivered to the solution. Unexpectedly, the sum of NO and NO_2 only reached 90 % of the HONO input in all three control experiments, indicating an additional loss mechanism for HONO that did not generate NO or NO_2. Since the observation was reproducible and only observed in the absence of a reactive sink in our positive control, it was possible to proceed with mass balance reaction experiments with the BODIPY-NH_2.

An aqueous solution of BODIPY-NH_2 containing 1 M HCl sampled gaseous HONO (25±14 ppbv) from our calibration source over three days (to minimize loss of the probe, see above). Fig 8 shows the absorbance change during sampling, while a time series of the HONO uptake as measured by the NO_x analyzer is given in Fig 9.

The observed UV-Vis absorption spectra for this experiment (Fig 8) had a similar pattern to our previous experiment with lower HONO mixing ratios (Fig 6, 2-4 ppbv). The same shoulder was observed at higher wavelengths with increasing HONO sampling duration. A notable difference was that the total absorbance in Fig 8 was not markedly reduced after sampling HONO for 61 hours.

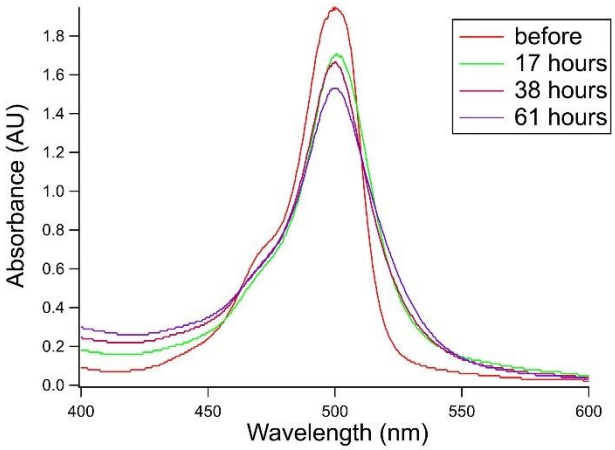

Fig 8. Change in the absorbance of BODIPY-NH_2 in 1 M HCl over time when bubbled with 25±14 ppbv of HONO measured with Ocean Optics Flame spectrometer.

As the sample probe loss was minimal, we then proceeded to calculate a mass balance of sampled HONO relative to the amount of probe present in solution, following the same calculation that was validated with our aniline positive control. Briefly, the HONO input to the bubbler was assumed to be the reading of the NO_2 channel during measurements of the calibration source output (E1). Our custom HONO calibration source has previously been shown to only have NO impurities, which are

View Article Online
DOI: 10.1039/D1AN01088A

within 10% of the output, and that HONO is quantitatively detected by this instrumental setup.[60] The uptake of HONO was then calculated (E2). A detailed treatment of the mass balance calculation is available in the Supporting Information (Section S2).

$$\mathbf{HONO}_{\mathbf{in}} = \mathbf{HONO}_{\mathbf{cs}} \quad \text{(E1)}$$

$$\mathbf{HONO}_{\mathbf{uptake}} = \mathbf{HONO}_{\mathbf{in}} - [(\mathbf{NO}_{\mathbf{output}} + (\mathbf{HONO} + \mathbf{NO_2}_{\mathbf{output}})) - \mathbf{NO}_{\mathbf{cs}}] \quad \text{(E2)}$$

Where $HONO_{in}$ refers to HONO input to the BODIPY-NH_2 sampling solution and $HONO_{cs}$ is the HONO measurement of the calibration source on the NO_x analyzer. The NO_{output} and $HONO + NO_{2\ output}$ are NO and HONO + NO_2 measurement exiting the impinger, as measured by the NO_x analyzer, respectively. $HONO_{uptake}$ refers to the HONO that is lost to the sampling solution in the reaction of probe with HONO.

The uncertainties of the calculated uptake quantity are dominated by the precision of the HONO output from the calibration source when fitted with a salt bed, which can vary in precision from 10-30% in previous work.[60] We used the maximum of this range as an upper limit to estimate the uncertainty in the HONO calibration source output. Any missing mass in the nitrogen mass balance was assumed to correspond to the formation of N_2 via diazotization[59] and the previously discussed decomposition pathway. Identifying the reaction endpoint is challenging, as the exact point where NO and NO_2 produced from R5 reach steady state can be masked by equilibrium processes, which increased the uncertainty. To reduce this, we selected the time where the NO_2 measurement in the output began to increase as an indication of reaction being near completion.

From Fig 9, the uptake of gas-phase HONO by the probe was quantitative initially (0-800 mins) as indicated by measured HONO + NO_2 exiting the bubbler being less than 0.04 of the HONO input. At approximately 800 min (Fig 9), the NO_2 and NO exiting the bubbler were observed to rise. This suggests that the reaction of the probe with HONO was near completion and any unreacted was being observed exiting in the bubbler gas flow. At 900 min, through integration of E2 over time, we calculated a total of 1.36(±0.40)x10^{-6} moles of HONO sampled, corresponding to 95±30% of the total amount of BODIPY probe in the solution (1.43x10^{-6} moles), again within the expected 10-30% precision of the modified HONO source.[60] This is in agreement with the mass spectrometry results (Fig S20) in which no ions at m/z 498.08 corresponding to BODIPY-NH_2 mass were detected. This therefore suggests that the probe was fully converted to products at the end of the experiment.

Once the reaction of our probe was complete, the HONO bubbled into solution either passes through or follows R4 or R5. Due to the reaction matrix consisting of 1 M HCl (pH=0), R5 is expected to be a negligible pathway and HONO loss should instead be dominated by R6. After 2000 min (Fig 9), the impinger output reached a steady state with the levels of NO and HONO + NO_2 at 0.2-0.3 and 0.4-0.5 fraction of HONO input, respectively, and consistent with the observations of our control experiments.

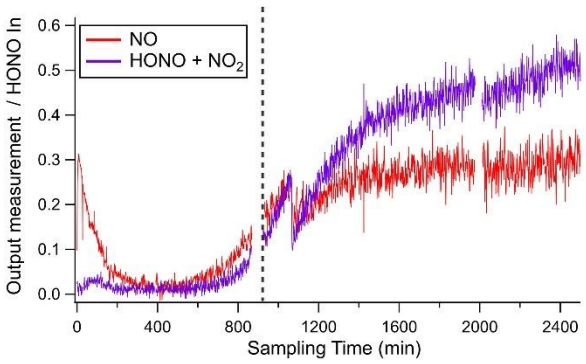

Fig 9 Time series of measured HONO+ NO_2 and NO in the impinger output as a fraction of the HONO input when 31.5 μg mL^{-1} BODIPY-NH_2 in 1 M HCl solution sampled gas-phase HONO (25±14 ppbv). NO measurement was corrected for the NO impurities from calibration source. Gaps in the time series are due to background measurements. Dashed line at 900 min indicates the time used for mass balance calculation.

The above experiments were performed under controlled conditions (i.e., using zero air) and therefore we next examined the ability of the probe to sample HONO in a matrix of indoor air. For this experiment, the indoor air was first scrubbed of any ambient HONO using a denuder coated with Na_2CO_3 and then HONO of a known mixing ratio (17± 0.2 ppbv) was added to the indoor air using the calibration source prior to sampling with the probe (31.5 μg mL^{-1} solution of BODIPY-NH_2 in 1 M HCl). This was to ensure a consistent known amount of HONO was added during this experiment and so that mass balance calculations could be utilized, while not excluding potential ambient interferences such as NO_2 (present at 10-20 ppbv during the experiments, R2). The sampling setup is shown in Fig S24. Fig 10 demonstrates that in indoor air HONO

was taken up by the solution, with the observed change in absorbance similar to the control experiments (Fig 8).

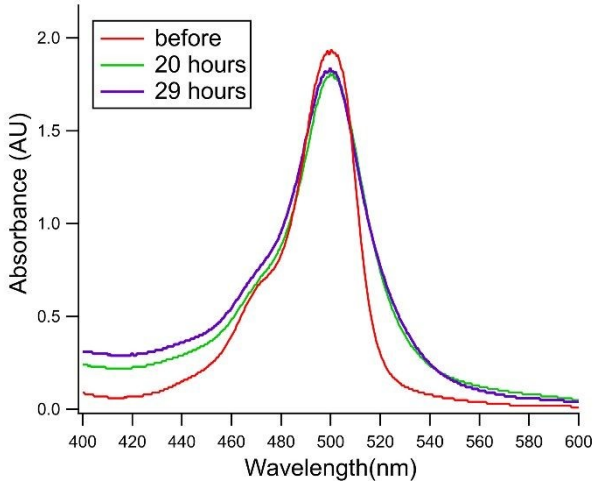

Fig 10. Change in the absorbance of BODIPY-NH_2 in 1 M HCl over time when bubbled with 17± 0.2 ppbv of HONO added to acid-free room air measured with Ocean Optics Flame spectrometer.

Fig 11 presents the time series of measured NO_x from the output of the BODIPY-NH_2 in 1 M HCl solution during the indoor air sampling. For this experiment the mass balance calculation has higher uncertainty compared to the controlled experiments due to the presence and variability of NO_x levels in the sampled indoor air. However, in the absence of a combustion source, most of the NO_x indoors will be NO_2 and therefore the increase in NO in the outflow of the sampling solution was indicative that the reaction was near completion. This change in NO was observed after approximately 1200 minutes (20 hours) of sampling (Fig 11). The reaction nearing the stoichiometric endpoint is further confirmed by the measured change in the UV-Vis absorbance at this time (Fig 10, 20 hours). Overall, Figs 10 and 11 demonstrate that a solution of BODIPY-NH_2 in 1 M HCl can sample HONO in the presence of matrix components typically found in a sample of ambient indoor air. This specifically suggests that cross-reactivity in the presence of 10-20 ppbv NO_x, mostly as NO_2, is undetectable in these experiments and therefore minor in nature.

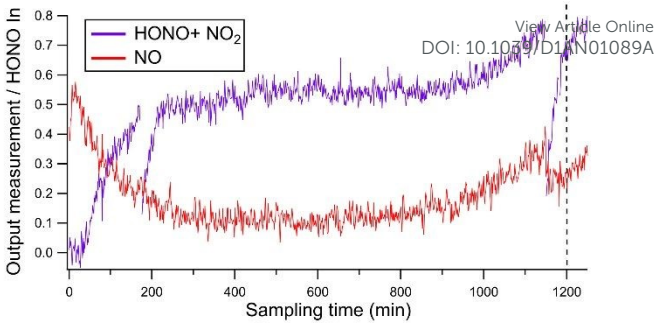

Fig 11 Time series of measured HONO+ NO_2 and NO in the impinger output as a fraction of the HONO input when 31.5 µg/mL BODIPY-NH_2 in 1 M HCl solution sampled gas-phase HONO (25±14 ppbv). NO measurement was corrected for the NO impurities from calibration source. Dashed line at 1200 min indicates the time used for the absorbance measurement.

Conclusions

In this work, we present a sensitive boron dipyrromethene based probe (2,6-disodiumsulfonyl-1,3,7,9-tetramethyl-5-(4-aminophenyl)-BODIPY; BODIPY-NH_2) for sampling gaseous HONO. The synthesis of the BODIPY-NH_2 probe is described and confirmed with NMR spectroscopy. The BODIPY probe reactivity was first tested using an acidic solution and sodium nitrite in excess as a source of in-situ nitrous acid. The reaction proceeded readily to completion on a timescale of 10 minutes. Characterization of the products from this reaction by high resolution mass spectrometry indicated diazotization to be the likely reaction mechanism. The probe and the products all displayed a high molar extinction coefficient, with the probe being fluorescent in acidic aqueous solution (Φ=33%) which turns off after reaction with HONO (Φ=0%; see Fig S17). These optical properties indicate viable use of UV-Vis spectrometry to measure HONO via this probe or its products at atmospherically relevant concentrations in the indoor environment (i.e. ppbv range) with high sensitivity.

The demonstrated fast pseudo-first-order reaction kinetics ($k=7.7\times10^{-4}$ s^{-1}) between the BODIPY probe and HONO, without any measurable intermediates, indicates its suitability for passive sampling in the ambient atmosphere. The rate is not so fast as to create a diffusion limitation in gas sampling, which is ideal for avoiding established issues in target gas collection rates (e.g. air movement from wind or HVAC). We demonstrated that the BODIPY probe would also react quantitatively with gaseous HONO. Mass balance

View Article Online
DOI: 10.1039/D1AN01289A

calculations between the amount of probe available and the amount HONO sampled further indicated quantitative uptake and was confirmed by a series of control experiments.

Overall, this work has provided proof-of-concept for using the BODIPY-NH_3^+ probe to quantitatively measure gaseous HONO concentrations in ambient air. The use of this probe overcomes current limitations in the indoor air quality and exposure passive sampling community. First, we expect the high molar absorptivity enables sensitive detection of HONO at ambient levels in reasonable deployment periods (e.g. days). Second, it is amenable to quantitative detection by many existing analytical instrumentation strategies. Since the suite of product molecules have different hydrophobicity, the potential of this probe could be maximized by combining it with separation techniques**.** Last, it is selective for the collection of HONO, allowing it to be quantified, and future NO_x measurements by passive techniques to be corrected for the known interference presented by HONO. The probe could therefore be coated on reactive pads and used in diffusive passive samplers for indoor air quality studies. This will be the focus of future work.

Conflicts of interest

There are no conflicts to declare.

Author Contributions

TV and CC supervised the experiments, acquired the funding, and provided resources to support this work. TV JB and CC conceptualized the molecular probe. JB synthesized and characterized the probe by NMR. DNF conducted all reactions and characterizations by UV-Vis, UHRMS, and with the NOx analyzer, including data analysis and visualization. LC aided in the setup of gas sampling experiments and data analysis. DNF created the schematics and reaction mechanisms and prepared the manuscript with contributions from all authors. All authors participated in data analysis and the review and editing of the manuscript.

Acknowledgments

Financial support for this work was provided by the Alfred P. Sloan Foundation Chemistry of Indoor Environments Program (G-2018-1051). TCV and CBC declare research support by NSERC Discovery Grants (RGPIN-2020-06166 and RGPIN-2018-05827 and TCV by the Early Career Researcher Discovery Launch Supplement (DGECR-2020-00186). We thank Howard N. Hunter for assistance with the NMR measurements. We thank Dr. Thomas Baumgartner for access to and help with the spectroscopic measurements Edinburgh instruments. We acknowledge the help of Dr. Joshua Gaffen and Amy Laturski with setting up and operating the Edinburgh instruments. We thank Carolyn E. Hempstead for the loan of the Ocean Optics spectrometer and Melodie Lao for their help with the HONO calibration source.

Notes and references

1 Y. B. Lim and P. J. Ziemann, *Environ. Sci. Technol.*, 2009, **43**, 2328–2334.

2 A. T. Lambe, T. B. Onasch, D. R. Croasdale, J. P. Wright, A. T. Martin, J. P. Franklin, P. Massoli, J. H. Kroll, M. R. Canagaratna, W. H. Brune, D. R. Worsnop and P. Davidovits, *Environ. Sci. Technol.*, 2012, **46**, 5430–5437.

3 L. R. Crilley, L. J. Kramer, B. Ouyang, J. Duan, W. Zhang, S. Tong, M. Ge, K. Tang, M. Qin, P. Xie, M. D. Shaw, A. C. Lewis, A. Mehra, T. J. Bannan, S. D. Worrall, M. Priestley, A. Bacak, H. Coe, J. Allan, C. J. Percival, O. A. M. Popoola, R. L. Jones and W. J. Bloss, *Atmos. Meas. Tech.*, 2019, **12**, 6449–6463.

4 S. Zhou, C. J. Young, T. C. VandenBoer, S. F. Kowal and T. F. Kahan, *Environ. Sci. Technol.*, 2018, **52**, 8355–8364.

5 S. Gligorovski, *J. Photochem. Photobiol. A Chem.*, 2016, **314**, 1–5.

6 V. Bartolomei, E. Gomez Alvarez, J. Wittmer, S. Tlili, R. Strekowski, B. Temime-Roussel, E. Quivet, H. Wortham, C. Zetzsch, J. Kleffmann and S. Gligorovski, *Environ. Sci. Technol.*, 2015, 49, 6599–6607.

7 C. J. Young, S. Zhou, J. A. Siegel and T. F. Kahan, *Environ. Sci. Process. Impacts*, 2019, **21**, 1229–1239.

8 J. Kleffmann, *ChemPhysChem*, 2007, **8**, 1137–1144.

9 R. Volkamer, P. Sheehy, L. T. Molina and M. J. Molina, *Atmos. Chem. Phys.*, 2010, **10**, 6969–6991.

10 S. Kim, T. C. VandenBoer, C. J. Young, T. P. Riedel, J. A. Thornton, B. Swarthout, B. Sive, B. Lerner, J. B. Gilman, C. Warneke, J. M. Roberts, A. Guenther, N. L. Wagner, W. P. Dubé, E. Williams and S. S. Brown, *J. Geophys. Res. Atmos.*, 2014, **119**, 6886–6896.

11 C. J. Young, R. A. Washenfelder, J. M. Roberts, L. H. Mielke, H. D. Osthoff, C. Tsai, O. Pikelnaya, J. Stutz, P. R. Veres, A. K. Cochran, T. C. Vandenboer, J. Flynn, N. Grossberg, C. L. Haman, B. Lefer, H. Stark, M. Graus, J. De Gouw, J. B. Gilman, W. C. Kuster and S. S. Brown, *Environ. Sci. Technol.*, 2012, **46**, 10965–10973.

12 J. Zhang, J. Chen, C. Xue, H. Chen, Q. Zhang, X. Liu, Y. Mu, Y. Guo, D. Wang, Y. Chen, J. Li, Y. Qu and J. An, *Sci. Total Environ.*, 2019, **681**, 110–123.

13 J. Stutz, H. J. Oh, S. I. Whitlow, C. Anderson, J. E. Dibb, J. H. Flynn, B. Rappenglück and B. Lefer, *Atmos. Environ.*, 2010,

44, 4090–4098.

14 J. Heland, J. Kleffmann, R. Kurtenbach and P. Wiesen, *Environ. Sci. Technol.*, 2001, **35**, 3207–3212.

15 B. J. Finlayson-Pitts, L. M. Wingen, A. L. Sumner, D. Syomin and K. A. Ramazan, *Phys. Chem. Chem. Phys.*, 2003, **5**, 223–242.

16 W. Yang, C. Han, H. Yang and X. Xue, *Environ. Pollut.*, 2018, **243**, 679–686.

17 A. F. Khalizov, M. Cruz-Quinones and R. Zhang, *J. Phys. Chem. A*, 2010, **114**, 7516–7524.

18 R. Kurtenbach, K. H. Becker, J. A. G. Gomes, J. Kleffmann, J. C. Lörzer, M. Spittler, P. Wiesen, R. Ackermann, A. Geyer and U. Platt, *Atmos. Environ.*, 2001, **35**, 3385–3394.

19 J. G. Calvert, G. Yarwood and A. M. Dunker, *Res. Chem. Intermed.*, 1994, **20**, 463–502.

20 Q. Yang, H. Su, X. Li, Y. Cheng, K. Lu, P. Cheng, J. Gu, S. Guo, M. Hu, L. Zeng, T. Zhu and Y. Zhang, *Sci. China Chem.*, 2014, **57**, 1032–1042.

21 Z. Xu, T. Wang, J. Wu, L. Xue, J. Chan, Q. Zha, S. Zhou, P. K. K. Louie and C. W. Y. Luk, *Atmos. Environ.*, 2015, **106**, 100–109.

22 V. Selimovic, R. J. Yokelson, C. Warneke, J. M. Roberts, J. A. de Gouw and D. W. T. Griffith, *Atmos. Chem. Phys.*, 2018, **18**, 2929–2948.

23 R. M. Mushinski, R. P. Phillips, Z. C. Payne, R. B. Abney, I. Jo, S. Fei, S. E. Pusede, J. R. White, D. B. Rusch and J. D. Raff, *Proc. Natl. Acad. Sci.*, 2019, **116**, 2138–2145.

24 P. Veres, J. M. Roberts, I. R. Burling, C. Warneke, J. De Gouw and R. J. Yokelson, *J. Geophys. Res. Atmos.*, 2010, 115.

25 R. Oswald, T. Behrendt, M. Ermel, D. Wu, H. Su, Y. Cheng, C. Breuninger, A. Moravek, E. Mougin, C. Delon, B. Loubet, A. Pommerening-Röser, M. Sörgel, U. Pöschl, T. Hoffmann, M. O. Andreae, F. X. Meixner and I. Trebs, *Science (80-.).*, 2013, **341**, 1233–1235.

26 L. Kramer, L. Crilley, T. Adams, S. Ball, F. Pope and W. Bloss, *Atmos. Chem. Phys. Discuss.*, 2019, 1–31.

27 D. B. Collins, R. F. Hems, S. Zhou, C. Wang, E. Grignon, M. Alavy, J. A. Siegel and J. P. D. Abbatt, *Environ. Sci. Technol.*, 2018, **52**, 12419–12427.

28 K. Lee, J. Xue, A. S. Geyh, H. Özkaynak, B. P. Leaderer, C. J. Weschler and J. D. Spengler, *Environ. Health Perspect.*, 2002, **110**, 145–149.

29 B. P. Leaderer, L. Naeher, T. Jankun, K. Balenger, T. R. Holford, C. Toth, J. Sullivan, J. M. Wolfson and P. Koutrakis, *Environ. Health Perspect.*, 1999, **107**, 223–231.

30 A. Febo and C. Perrino, *Atmos. Environ. Part A, Gen. Top.*, 1991, **25**, 1055–1061.

31 T. C. VandenBoer, S. S. Brown, J. G. Murphy, W. C. Keene, C. J. Young, A. A. P. Pszenny, S. Kim, C. Warneke, J. A. de Gouw, J. R. Maben, N. L. Wagner, T. P. Riedel, J. A. Thornton, D. E. Wolfe, W. P. Dubé, F. Öztürk, C. A. Brock, N. Grossberg, B. Lefer, B. Lerner, A. M. Middlebrook and J. M. Roberts, *J. Geophys. Res. Atmos.*, 2013, **118**, 10,155-10,171.

32 K. W. Wong, B. L. Lefer, B. Rappenglück and J. Stutz, *Atmos. Chem. Phys.*, 2011, **11**, 3595–3609.

33 Government of Canada, Residential Indoor Air Quality Guideline: Nitrogen Dioxide, https://www.canada.ca/en/health-canada/services/publications/healthy-living/residential-indoor-air-quality-guideline-nitrogen-dioxide.html.

34 E. Gómez Alvarez, M. Sörgel, S. Gligorovski, S. Bassil, V. Bartolomei, B. Coulomb, C. Zetzsch and H. Wortham, *Atmos. Environ.*, 2014, **95**, 391–399.

35 C. W. Spicer, R. W. Coutant, G. F. Ward, D. W. Joseph, A. J. Gaynor and I. H. Billick, *Environ. Int.*, 1989, **15**, 643–654.

36 T. Wainman, C. J. Weschler, P. J. Lioy and J. Zhang, *Environ. Sci. Technol.*, 2001, **35**, 2200–2206.

37 J. Kleffmann, K. H. Becker and P. Wiesen, *Atmos. Environ.*, 1998, **32**, 2721–2729.

38 J. N. Pitts, D. Grosjean, K. Van Cauwenberghe, J. P. Schmid and D. R. Fitz, *Environ. Sci. Technol.*, 1978, **12**, 946–953.

39 M. Sleiman, L. A. Gundel, J. F. Pankow, P. Jacob, B. C. Singer and H. Destaillats, *Proc. Natl. Acad. Sci. U. S. A.*, 2010, **107**, 6576–6581.

40 T. C. Vandenboer, C. J. Young, R. K. Talukdar, M. Z. Markovic, S. S. Brown, J. M. Roberts and J. G. Murphy, *Nat. Geosci.*, 2015, **8**, 55–60.

41 G. Huang, X. Zhou, G. Deng, H. Qiao and K. Civerolo, *Atmos. Environ.*, 2002, **36**, 2225–2235.

42 C. Afif, C. Jambert, V. Michoud, A. Colomb, G. Eyglunent, A. Borbon, V. Daële, J. F. Doussin and P. Perros, *J. Environ. Sci. (China)*, 2016, **40**, 105–113.

43 U. Platt, D. Perner, G. W. Harris, A. M. Winer and J. N. Pitts, *Nature*, 1980, **285**, 312–314.

44 A. A. Salem, A. A. Soliman and I. A. El-Haty, *Air Qual. Atmos. Heal.*, 2009, **2**, 133–145.

45 T. Górecki and J. Namienik, *TrAC - Trends Anal. Chem.*, 2002, **21**, 276–291.

46 F. Wania and C. Shunthirasingham, *Environ. Sci. Process. Impacts*, 2020, **22**, 1925–2002.

47 R. M. Cox, *Environ. Pollut.*, 2003, **126**, 301–311.

48 M. R. Heal, D. P. H. Laxen and B. B. Marner, *Atmosphere (Basel).*, 2019, **10**, 1–28.

49 A. Loudet and K. Burgess, *Chem. Rev.*, 2007, **107**, 4891–4932.

50 T. Ehrenschwender and H. Wagenknecht, 1–13.

51 N. Dorh, S. Zhu, K. B. Dhungana, R. Pati, F. T. Luo, H. Liu and A. Tiwari, *Sci. Rep.*, 2015, **5**, 1–10.

52 N. Boens, V. Leen and W. Dehaen, *Chem. Soc. Rev.*, 2012, **41**, 1130–1172.

53 L. Li, J. Han, B. Nguyen and K. Burgess, *J. Org. Chem.*, 2008, **73**, 1963–1970.

54 A. Treibs and F. -H Kreuzer, *Justus Liebigs Ann. Chem.*, 1968, 718, 208–223.

55 B. Gu, L. Huang, J. Hu, J. Liu, W. Su, X. Duan, H. Li and S. Yao, *Talanta*, 2016, **152**, 155–161.

56 N. Adarsh, M. Shanmugasundaram and D. Ramaiah, *Anal. Chem.*, 2013, **85**, 10008–10012.

57 K. J. Huang, W. Z. Xie, H. S. Zhang and H. Wang, *Microchim. Acta*, 2008, **161**, 201–207.

58 J. Zhang, F. Pan, Y. Jin, N. Wang, J. He, W. Zhang and W. Zhao, *Dye. Pigment.*, 2018, **155**, 276–283.

View Article Online
DOI: 10.1039/D1AN01089A

59 H. Zollinger, *Diazo Chemistry I Diazo Chemistry I: Aromatic and Heteroaromatic Compounds. By Heinrich Zollinger Copyright © 1994 VCH Vertagsgesellschaft mbH*, 1994.

60 M. Lao, L. R. Crilley, L. Salehpoor, T. C. Furlani, I. Bourgeois, J. Andrew Neuman, A. W. Rollins, P. R. Veres, R. A. Washenfelder, C. C. Womack, C. J. Young and T. C. Vandenboer, *Atmos. Meas. Tech.*, 2020, **13**, 5873–5890.